

## PAPER

[View Article Online](#)  
[View Journal](#) | [View Issue](#)Cite this: *J. Mater. Chem. A*, 2024, 12, 31526Glycidol-modified PEI: a highly selective adsorbent for SO<sub>2</sub> in the presence of CO<sub>2</sub><sup>†</sup>Chanjot Kaur  and Abdelhamid Sayari \*

Amine-containing CO<sub>2</sub> adsorbents are highly sensitive to the presence of SO<sub>2</sub> in the feed gas, even in minute amounts. It is thus necessary to remove SO<sub>2</sub> quantitatively prior to CO<sub>2</sub> capture. To this end, we developed a silica-supported polyethylenimine (GD-PEI/S) adsorbent containing only tertiary amines *via* quantitative glycidol functionalization. The novel material was characterized by infra-red (IR) and nuclear magnetic resonance (NMR) spectroscopy, and by thermogravimetric analysis (TGA). In the presence of a gas mixture containing 5 ppm SO<sub>2</sub> and more than a  $2 \times 10^4$  higher concentration of CO<sub>2</sub>, the GD-PEI/S material adsorbed SO<sub>2</sub> quantitatively until near saturation, with no CO<sub>2</sub> uptake, indicating that the adsorbent exhibits 100% SO<sub>2</sub> selectivity *versus* CO<sub>2</sub>, even in the presence of very high CO<sub>2</sub>/SO<sub>2</sub> ratios. Furthermore, the SO<sub>2</sub> uptake of the adsorbent almost doubled in the presence of humidity, possibly due to increased diffusion of SO<sub>2</sub>. Under recycling conditions, GD-PEI/S showed good reversibility in the presence of both dry and humid SO<sub>2</sub> at low and high SO<sub>2</sub> concentrations.

Received 19th August 2024  
Accepted 8th October 2024

DOI: 10.1039/d4ta05829a

[rsc.li/materials-a](https://rsc.li/materials-a)

## 1. Introduction

As the main contributor to the greenhouse gas effect, CO<sub>2</sub> plays a predominant role in global warming.<sup>1</sup> The National Oceanic and Atmospheric Administration (NOAA) reported increasing levels of CO<sub>2</sub> in the atmosphere reaching 422 ppm in 2024.<sup>2</sup> Increasing levels of CO<sub>2</sub> in the atmosphere were correlated with the increase in earth's temperature.<sup>3</sup> CO<sub>2</sub> capture and sequestration from flue gas and directly from air, is recognized as a key strategy for reducing CO<sub>2</sub> emissions, from stationary and distributed sources.<sup>4,5</sup>

Regarding CO<sub>2</sub> capture, solid amine adsorbents received significant attention due to their excellent selectivity, high adsorption capacity and low energy regeneration.<sup>6–8</sup> Nevertheless, there are challenges in using solid amine adsorbents, including the deleterious effect of harmful acidic gas impurities, such as SO<sub>x</sub> and NO<sub>x</sub>, that may occur in flue gas. Such species not only cause environmental and health issues but are detrimental to CO<sub>2</sub> capture due to their strongly competitive adsorption.<sup>9</sup> Note that, due to the potential health risks and environmental impact associated with elevated concentrations of SO<sub>2</sub> in the atmosphere,<sup>10</sup> limits are imposed on sulfur emissions from large power facilities. Typical mandatory limits for SO<sub>2</sub> in exhaust gases are set to 120 ppm in the US, 75 to 300 ppm in China, and 50 to 250 ppm in Europe.<sup>11</sup> However, no matter how low the residual SO<sub>2</sub> content in the feed gas, amines

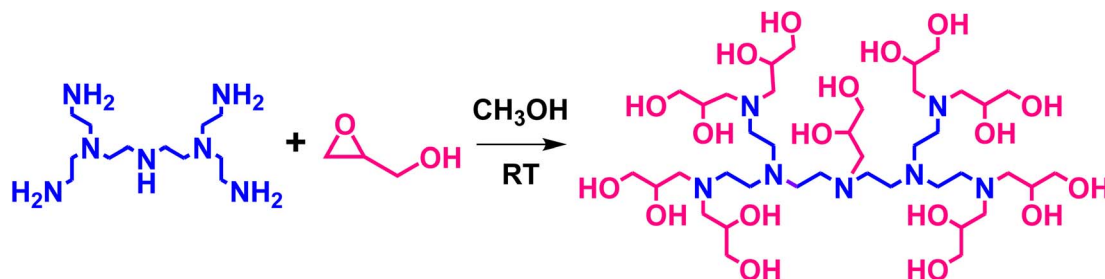
in CO<sub>2</sub> adsorbents will be irreversibly deactivated.<sup>12–14</sup> For example, Jones and co-workers<sup>14</sup> reported that when a PEI-impregnated silica support was exposed to a mixture of 20 ppm SO<sub>2</sub>, 10% CO<sub>2</sub> balance N<sub>2</sub> at 35 °C, the adsorbent lost 41% of CO<sub>2</sub> uptake after the first cycle of adsorption. Therefore, before adsorbing CO<sub>2</sub> on amine-containing materials, it is crucial to remove SO<sub>2</sub> quantitatively from the feed gas.

Although there are numerous technologies for flue gas desulfurization, particularly liquid phase scrubbing,<sup>15</sup> work on selective removal of traces of SO<sub>2</sub> in the presence of much higher CO<sub>2</sub> partial pressures is more pertinent for carbon capture over amine-containing adsorbents. More specifically, meeting this objective using adsorption would be easier to streamline with processes of CO<sub>2</sub> capture by adsorption. Many candidate materials were proposed for SO<sub>2</sub> removal, including metal organic frameworks (MOFs),<sup>16,17</sup> zeolites,<sup>18,19</sup> porous polymers<sup>20–22</sup> and activated carbons.<sup>23,24</sup> Nonetheless, they have limitations; for example, activated carbons showed very limited selectivity and efficiency<sup>25</sup> in the presence of O<sub>2</sub> and H<sub>2</sub>O, as they deactivated, producing H<sub>2</sub>SO<sub>4</sub>.<sup>26</sup> A number of MOFs with SO<sub>2</sub> *vs.* CO<sub>2</sub> selectivity between 28 and 44 were reported in the literature.<sup>27–29</sup> However, not only are such selectivities not high enough, but the SO<sub>2</sub> concentration used was somewhat high ( $\geq 2000$  ppm).

Adsorbents containing only tertiary amines seem to be the most selective for SO<sub>2</sub> *vs.* CO<sub>2</sub>. Tertiary amines adsorb SO<sub>2</sub> readily, but do not interact with CO<sub>2</sub>, at least under dry conditions.<sup>14,30–39</sup> For instance, when Tailor and Sayari<sup>32</sup> exposed propyldiethanolamine grafted on a pore-expanded MCM-41 support to a 50 : 50 mixture of 0.1% SO<sub>2</sub> balance N<sub>2</sub> and 20% CO<sub>2</sub> balance He at room temperature, they found that the presence of CO<sub>2</sub> had no effect on the adsorbent's ability to

Centre for Catalysis Research and Innovation, Department of Chemistry and Biomolecular Sciences, University of Ottawa, Ottawa, Ontario K1N 6N5, Canada.  
E-mail: [abdel.sayari@uottawa.ca](mailto:abdel.sayari@uottawa.ca)

<sup>†</sup> Electronic supplementary information (ESI) available. See DOI: <https://doi.org/10.1039/d4ta05829a>



Scheme 1 Schematic of synthesis of GD-PEI.

adsorb  $\text{SO}_2$ . Also, the adsorbent could be fully regenerated after 11 adsorption–desorption cycles, which indicates high stability of the material against heat and  $\text{SO}_2$ .

However, achieving complete functionalization of PEI protic amines into tertiary amines was found to be either difficult<sup>33</sup> or tedious.<sup>30,35,36,38</sup> Moreover, the majority of reported studies focused on removing high levels of  $\text{SO}_2$  in gas mixtures,<sup>30–32,35,36</sup> and to the best of our knowledge, none of the studies dealt with  $\text{SO}_2$  concentrations below 50 ppm. Furthermore, in some cases, the working capacity of the adsorbent was found to decrease significantly in the presence of humid  $\text{SO}_2$ .<sup>32</sup>

The objective of this work was to develop a novel polytertiary amine adsorbent to selectively and quantitatively remove  $\text{SO}_2$  at concentrations as low as 5 ppm in the presence of a typical flue gas  $\text{CO}_2$  concentration of 10–15%. To this end, complete functionalization of PEI with GD was achieved as shown in Scheme 1. In addition to its straightforward preparation, the glycidol-functionalized amine adsorbent exhibited stable working capacity in the presence of both dry and humid  $\text{SO}_2$  at low and high  $\text{SO}_2$  concentrations. It is noteworthy that in addition to tertiary amines being highly selective to  $\text{SO}_2$  adsorption, it was reported that the occurrence of hydroxyethylene groups decreases the energy for regeneration and increases the reversibility of the adsorbent.<sup>33,40</sup>

## 2. Experimental section

### 2.1. Materials

Polyethylenimine (PEI, Mw 1200), glycidol (GD, 96%), fumed silica (Cab-O-Sil, M5), tetramethylammonium hydroxide (TMAOH, 25 wt% solution), cetyltrimethylammonium bromide (CTAB, 98%), *N,N*-dimethyldodecyl amine (DMDA, 97%), tetraethyl orthosilicate (TEOS, 98%) and deuterium oxide ( $\text{D}_2\text{O}$ , 99.9%) were obtained from Sigma-Aldrich. Sodium aluminate ( $\text{NaAlO}_2$ , 92%) was obtained from Strem Chemicals. Anhydrous methanol (99.8%) and ammonia solution (30 wt%) were obtained from Fischer. Chemicals were used as obtained. Ultra-high purity (99.999%) nitrogen, 15% or 20%  $\text{CO}_2$  in nitrogen and gas cylinders containing 20, 100 and 1000 ppm  $\text{SO}_2$  in  $\text{N}_2$ , were purchased from Messer Canada.

### 2.2. Preparation of GD-PEI

A pore-expanded aluminosilica (PE- $\text{AlSiO}_2$ ) support was prepared as reported elsewhere,<sup>41</sup> and further details are included in the

ESI (Fig. S1).<sup>†</sup> Functionalization of primary and secondary amines of PEI with GD was carried out as reported by Fan *et al.*<sup>42</sup> with slight modifications. Briefly, 2 g of PEI (44 mmol of N) was dissolved in 20 mL of anhydrous methanol under a nitrogen atmosphere. Then, 3.55 g (47.96 mmol) of GD was added dropwise, and the solution was stirred for 4 h. After removing excess methanol using a rotary evaporator, the product was precipitated with acetone, and then separated and dried in a vacuum oven at 70 °C overnight. The functionalized PEI, denoted as GD-PEI was impregnated onto PE- $\text{AlSiO}_2$  as follows. The obtained GD-PEI compound was dissolved in 30 mL of anhydrous methanol and stirred until complete dissolution. After that, 5.5 g of PE- $\text{AlSiO}_2$  was slowly added into the solution and the mixture was stirred until the solvent evaporated. The final material was dried in an oven at 80 °C for 3 h and referred to as GD-PEI/S. 0.5 g of PEI was dissolved in 15 mL of methanol. After that, 0.5 g of PE- $\text{AlSiO}_2$  was added and the mixture was stirred overnight followed by evaporation of the solvent in an oven at 70 °C for 6 h to obtain PEI/S. The overall loading of PEI/S and GD-PEI/S was fixed to 50 wt% with respect to the adsorbent.

### 2.3. Characterization

The pore structure of PE- $\text{AlSiO}_2$  was investigated by  $\text{N}_2$  adsorption measurements at  $-196$  °C using a 3Flex instrument (Micromeritics). The sample was pretreated in flowing  $\text{N}_2$  at 120 °C for 4 h. The specific surface area was determined using the Brunauer–Emmett–Teller (BET) method at relative pressures ranging from 0.06 to 0.2. The total pore volume was measured at  $P/P_0 = 0.99$ , whereas the pore size distribution was calculated using the Kruk–Jaroniec–Sayari method.<sup>43</sup>

PEI and GD-PEI were dissolved in  $\text{D}_2\text{O}$  and their  $^{13}\text{C}$  nuclear magnetic resonance (NMR) spectra were obtained using an AVIII 600 spectrometer set to 45° pulses, 40 scans, 90 second relaxation delay and an acquisition time of 0.999 seconds. Inverse-gated proton decoupling was used to avoid the nuclear Overhauser effect. Fourier transform infrared spectroscopy (FTIR) spectra were obtained using a Cary 630 FTIR instrument by Agilent.

### 2.4. Adsorption measurements

$\text{SO}_2$  adsorption measurements were carried out in a fixed bed reactor as shown in Fig. 1. In a typical experiment, 0.5–1 g of the sample was loaded into a 1 cm long stainless steel column with 0.42 cm inner diameter, and placed in a temperature-controlled

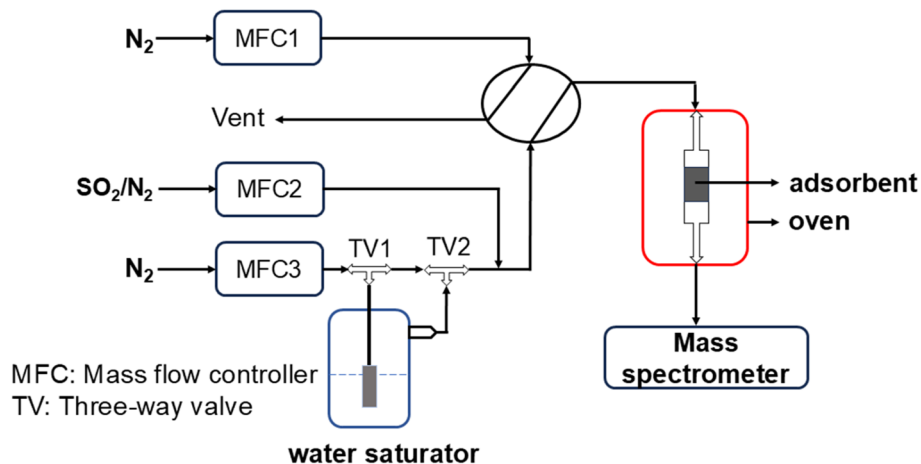


Fig. 1 Schematic of the column breakthrough setup.

oven. The material was pretreated under  $N_2$  ( $40 \text{ mL min}^{-1}$ ) at  $110^\circ\text{C}$  for 2 h. After cooling to  $23^\circ\text{C}$ , it was exposed to  $SO_2$  in a  $N_2$  gas mixture ( $40 \text{ mL min}^{-1}$ ) with different compositions. As for experiments under humid conditions,  $N_2$  was bubbled through a water saturator placed in a thermostatic bath maintained at  $20^\circ\text{C}$ , and then combined with the  $SO_2$  containing  $N_2$ . The gas mixture exiting the column was constantly analyzed by using a MKS Cirrus 3 mass spectrometer (MS), and breakthrough curves were obtained using MS data obtained for 64 amu. The  $SO_2$  adsorption capacity ( $\text{mmol g}^{-1}$ ) of GD-PEI/S at different partial pressures was calculated using eqn (1):

$$q = \frac{C_0 F t_q}{m} \quad (1)$$

where  $C_0$  is the inlet concentration of  $SO_2$ ,  $F$  is the flowrate of the gas mixture,  $m$  is the mass of the adsorbent and  $t_q$  is the stoichiometric time, which was evaluated from the column breakthrough curve using eqn (2):

$$t_q = \int_0^\infty \left(1 - \frac{C_A}{C_0}\right) dt \quad (2)$$

where  $C_A$  represents the downstream concentration of  $SO_2$ .

The  $CO_2$  uptake and organic content of GD-PEI/S were measured using a thermogravimetric analyzer (TGA 550, TA Instruments). The sample (*ca.* 20 mg) was pretreated under  $N_2$  for 60 min at  $110^\circ\text{C}$ , followed by cooling to  $25^\circ\text{C}$ , and then the gas stream was switched to 15%  $CO_2$  balance  $N_2$  for 30 min. After removal of adsorbed  $CO_2$ , if any, at  $110^\circ\text{C}$  for 10 min under flowing  $N_2$ , the adsorbent was cooled down to  $75^\circ\text{C}$ , and the gas stream was switched to 15%  $CO_2/N_2$  for 30 min. Then, the temperature was increased to  $700^\circ\text{C}$  at a rate of  $10^\circ\text{C min}^{-1}$  under flowing  $N_2$ , before switching the gas to air for 25 min. The organic content was determined as the weight loss of the material beyond  $200^\circ\text{C}$ .

### 3. Results and discussion

#### 3.1. Characterization of the adsorbent

The surface area, pore volume and average pore size of PE-AlSiO<sub>2</sub> were found to be  $818 \text{ m}^2 \text{ g}^{-1}$ ,  $1.66 \text{ cm}^3 \text{ g}^{-1}$  and  $8.13 \text{ nm}$ . According

to IUPAC nomenclature, the nitrogen adsorption-desorption isotherm of the support (Fig. 2a) was a Type IV isotherm, with an H1 hysteresis loop, indicating that the support is mesoporous. This is further confirmed by the pore size distribution shown in Fig. 2b, where the majority of pores fall within the range of 3–15 nm, with a maximum at 7 nm. The total polymer content of GD-PEI/S was 55 wt% with respect to the weight of the adsorbent (Fig. S2a†).

The FTIR spectra in Fig. 3 showed that the band at  $1567 \text{ cm}^{-1}$  in PEI/S corresponding to N–H bending<sup>44</sup> disappeared completely upon functionalization with GD. Moreover, the higher intensity hydroxyl band at  $3347 \text{ cm}^{-1}$  in GD-PEI/S compared to PEI/S is consistent with the significant increase of hydroxyl groups. Functionalization of PEI with GD was further confirmed using  $^{13}\text{C}$  NMR measurements as shown in Fig. 4. The carbon peaks were assigned as outlined in the literature.<sup>45,46</sup> Using the intensity of NMR peaks of carbon atoms adjacent to primary, secondary and tertiary amines in PEI, the percentage of such amines was found to be 36 : 37 : 27. Upon functionalization of PEI with GD, the NMR peaks corresponding to carbons neighboring primary and secondary amines disappeared, and new peaks attributable to carbons neighboring tertiary amines and to added GD, appeared (Scheme 1). This finding confirmed the incorporation of GD with complete conversion of primary and secondary amines into tertiary amines.

#### 3.2. $SO_2$ adsorption isotherm

Fig. 5 shows the  $SO_2$  uptake of GD-PEI/S at  $23^\circ\text{C}$  at different concentrations. The different gas compositions were achieved by diluting premixed 20, 100 or 1000 ppm  $SO_2/N_2$  with pure  $N_2$ , at different flowrates, while maintaining the overall flowrate at  $40 \text{ mL min}^{-1}$ . The shape of this isotherm is consistent with chemisorption. At low concentrations, the adsorption capacity increases steeply with increasing concentration, indicating the high sensitivity of tertiary amine groups toward  $SO_2$ . The uptake reaches a plateau at *ca.* 1000 ppm  $SO_2$ , presumably because most of the accessible adsorption sites are occupied. The actual  $SO_2$  uptakes *versus* partial pressure are listed in Table S1.† The breakthrough curves of GD-PEI/S under different partial pressures of  $SO_2$  are shown in Fig. S3.†

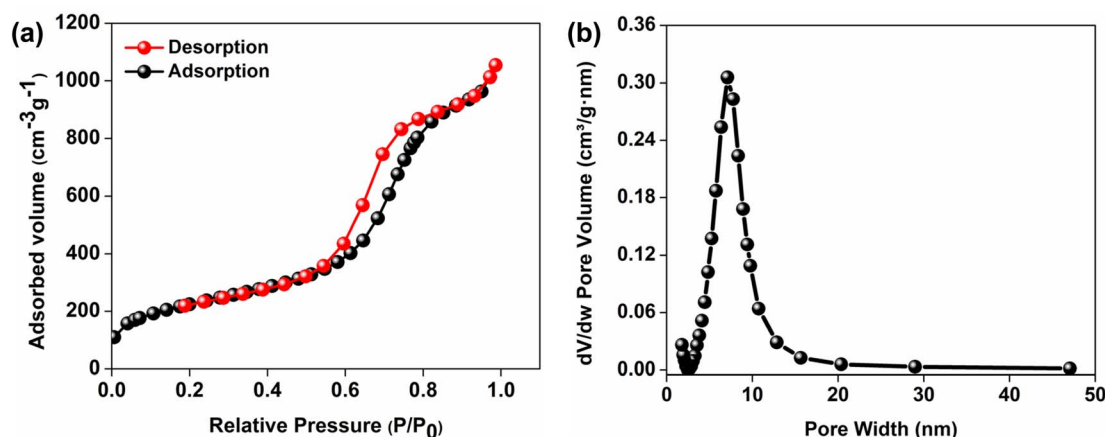


Fig. 2 (a)  $N_2$  adsorption-desorption isotherm and (b) pore size distribution of PE-AlSiO<sub>2</sub>.

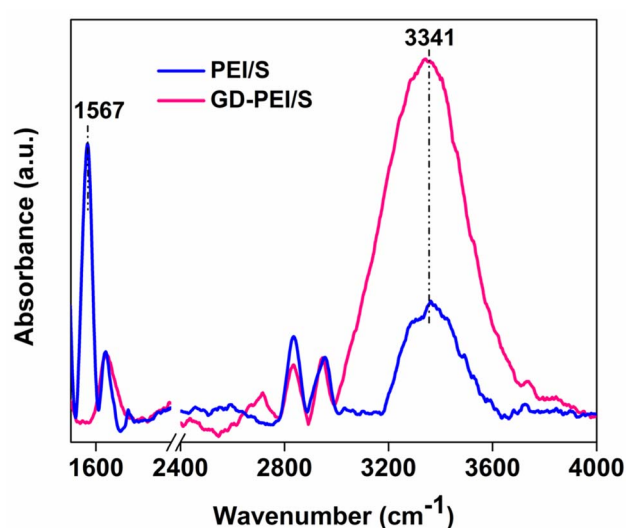


Fig. 3 FT-IR spectra of PEI/S and GD-PEI/S.

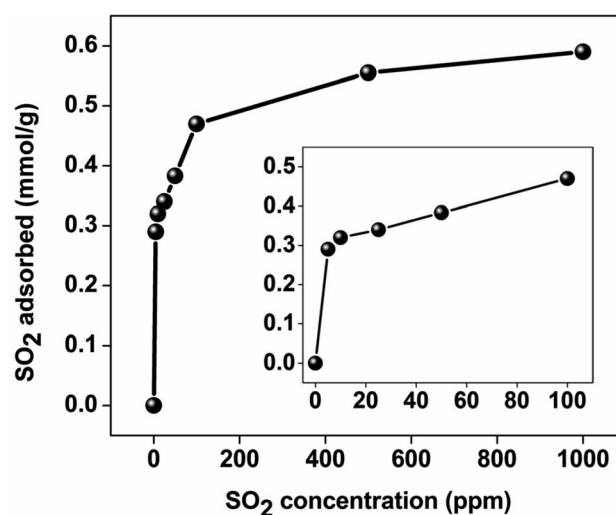


Fig. 5  $SO_2$  adsorption isotherms of GD-PEI/S.

### 3.3. Selectivity towards $SO_2$ versus $CO_2$

Fig. 6 depicts the column-breakthrough data over GD-PEI/S in the presence of 5 to 50 ppm  $SO_2$  in 10% or 11%  $CO_2$ , as

indicated. The gas compositions were achieved by mixing different concentrations of  $SO_2$  in  $N_2$  with 15% or 20% premixed  $CO_2$  in  $N_2$ , while maintaining the overall flowrate at 40 mL min<sup>-1</sup>. Column breakthrough curves showed that  $CO_2$  comes

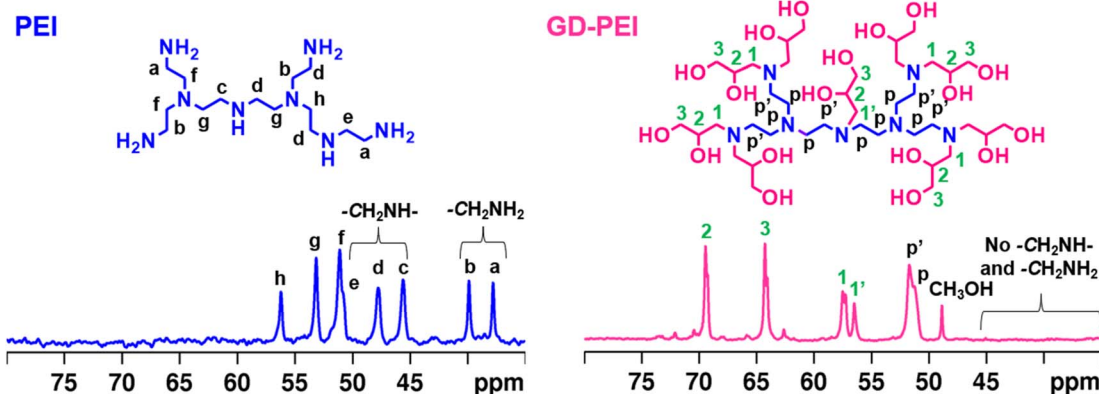


Fig. 4 <sup>13</sup>C NMR spectra of PEI and GD-PEI.



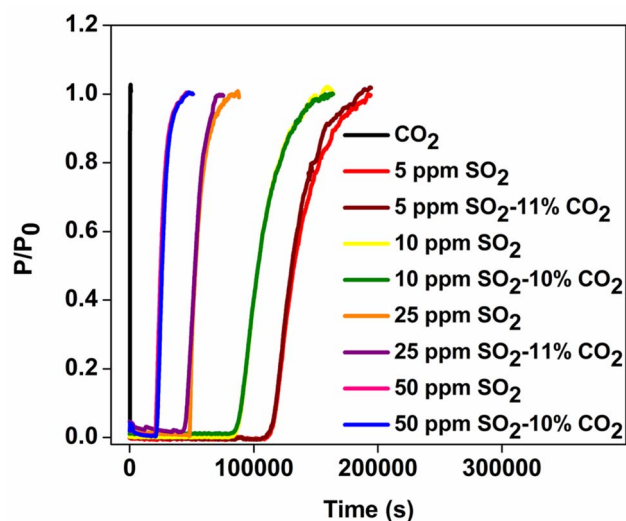


Fig. 6 Breakthrough curves of GD-PEI/S in the presence of different concentrations of SO<sub>2</sub> with and without CO<sub>2</sub>.

out of the column within few seconds of passing the gas mixture. Furthermore, regardless of the presence of CO<sub>2</sub>, the SO<sub>2</sub> uptake (Fig. S4<sup>†</sup>), breakthrough time, and equilibrium time remained the same at any given SO<sub>2</sub> concentration. This is consistent with TGA measurements (Fig. S2b<sup>†</sup>), which showed that the CO<sub>2</sub> uptake of GD-PEI/S was only 0.08 and 0.01 mmol g<sup>-1</sup> at 25 and 75 °C, respectively. These results indicate that no CO<sub>2</sub> was chemisorbed by GD-PEI/S, which is in line with the fact that under dry conditions, only protic amines interact with CO<sub>2</sub> to afford ammonium carbamate.<sup>47</sup>

### 3.4. Stability of the adsorbent under cycling conditions

To investigate the stability of SO<sub>2</sub> working capacity over GD-PEI/S or the lack thereof, a series of SO<sub>2</sub> adsorption-desorption cycles was carried out, with adsorption at 23 °C in the presence

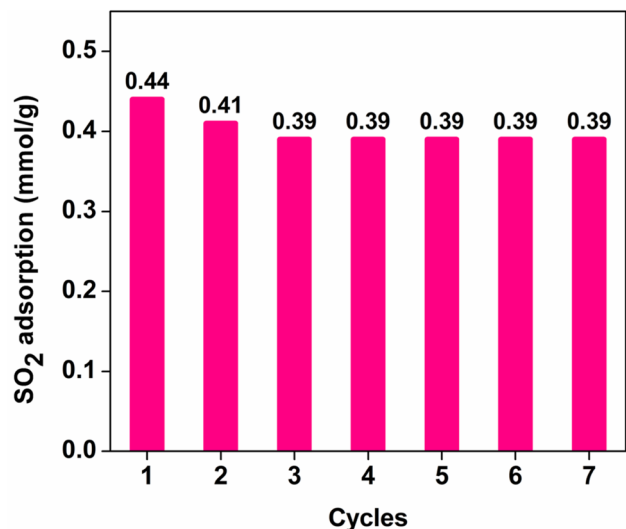


Fig. 7 Regeneration cycles of GD-PEI/S under dry 100 ppm SO<sub>2</sub> balance N<sub>2</sub>.

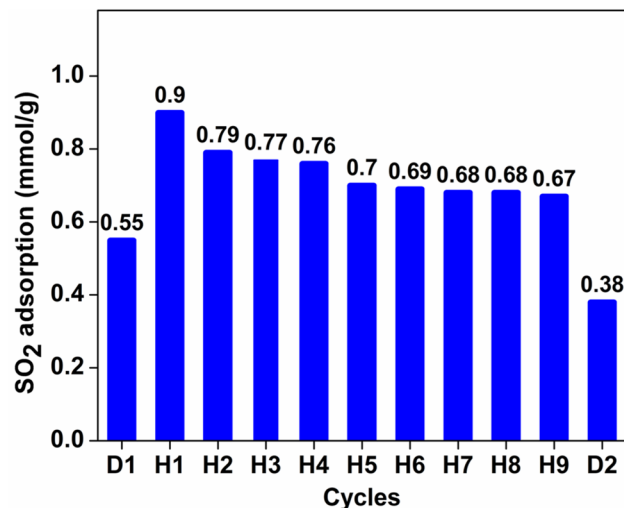
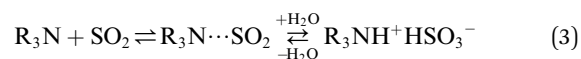


Fig. 8 Working capacity over GD-PEI/S of humid 500 ppm SO<sub>2</sub> in N<sub>2</sub>. D1 and D2 indicate data under dry conditions before and after the experiment under humid conditions.

of dry 100 ppm SO<sub>2</sub> in N<sub>2</sub>, and desorption at 110 °C in N<sub>2</sub>. SO<sub>2</sub> uptake of GD-PEI/S decreased by 7 and 5% during the first and second cycles, and then remained stable thereafter (Fig. 7). Moreover, breakthrough and equilibrium times remained the same after the second adsorption cycle, as seen in Fig. S5.<sup>†</sup> Zhu *et al.*<sup>38</sup> observed a similar trend and attributed the decrease in SO<sub>2</sub> uptake during the first cycle to the adsorption of SO<sub>2</sub> onto basic sites that were not completely regenerated.

Adsorption-desorption cycles were also performed under dry and humid 500 ppm SO<sub>2</sub> balance N<sub>2</sub> as shown in Fig. S6<sup>†</sup> and 8 respectively. In the absence of moisture, the adsorbent lost 17% SO<sub>2</sub> uptake after the first two regeneration cycles, and it remained almost stable in subsequent cycles. However, the adsorbent was deactivated more in 500 ppm SO<sub>2</sub> in N<sub>2</sub> than 100 ppm SO<sub>2</sub> in N<sub>2</sub>. This could be a result of elevated SO<sub>2</sub> concentration, which increases the interaction of SO<sub>2</sub> with adsorption sites and subsequently the likelihood of their deactivation. In agreement with other studies,<sup>30–32</sup> SO<sub>2</sub> adsorption capacity of GD-PEI/S increased by 64% under humid (42% RH) 500 ppm SO<sub>2</sub> in N<sub>2</sub>, from 0.55 to 0.90 mmol g<sup>-1</sup>, which may be because water can act as a lubricant, reducing the diffusion resistance for incoming SO<sub>2</sub>. Taylor *et al.*<sup>30</sup> proposed that this improvement may be due to the formation of ammonium bisulfite salt<sup>48,49</sup> in a humid environment as shown in eqn (3). Overall, the decrease in SO<sub>2</sub> uptake before stabilization was similar under dry and wet conditions *i.e.* ~23%. The corresponding breakthrough curves are shown in Fig. S7.<sup>†</sup>



## 4. Conclusion

GD-PEI/S was synthesized by converting all protic amines in PEI into tertiary amines using glycidol functionalization, followed

by impregnation onto pore-expanded  $\text{AlSiO}_2$ . The adsorbent showed a  $\text{SO}_2$  capacity of  $0.29 \text{ mmol g}^{-1}$  when exposed to 5 ppm  $\text{SO}_2/\text{N}_2$ , with a positive correlation with increasing  $\text{SO}_2$  concentration. The selectivity of the adsorbent towards  $\text{SO}_2$  was investigated in the presence of different concentrations of  $\text{SO}_2$  in  $\text{CO}_2/\text{N}_2$  mixtures. GD-PEI/S was found to be 100% selective for  $\text{SO}_2$  at concentrations as low as 5 ppm in the presence of 11%  $\text{CO}_2$ , corresponding to a  $\text{CO}_2/\text{SO}_2$  ratio of 22 000. The presence of only tertiary amines with no interaction with  $\text{CO}_2$  is at the origin of the high selectivity toward  $\text{SO}_2$  versus  $\text{CO}_2$ . Moreover, the adsorbent showed a more than two times increase in  $\text{SO}_2$  uptake under humid conditions. The adsorbent was also found to be stable during adsorption-desorption cycling in the presence of dry and wet  $\text{SO}_2/\text{N}_2$  mixtures. Therefore, GD-PEI/S may be used as a filter for extensive desulfurization before  $\text{CO}_2$  capture on amine-containing adsorbents.

## Data availability

The data supporting this article have been included as part of the ESI.† More data can be provided upon request.

## Author contributions

Chanjot Kaur: conceptualization, methodology, investigation, formal analysis, data curation, writing – original draft. Abdelhamid Sayari: conceptualization, supervision, writing (review and editing), funding acquisition.

## Conflicts of interest

There are no competing interests to declare.

## Acknowledgements

A. S. thanks the Natural Sciences and Engineering Research Council of Canada (NSERC) for a Discovery Grant (RGPIN-2024-06127).

## References

- 1 E. Kaur, M. Crippa, D. Guizzardi, F. Pagani, M. Banja, M. Muntean, E. Schaaf, W. Becker, F. Monforti-Ferrario, R. Quadrelli, A. Risquez Martin, P. Taghavi-Moharamli, J. Köykkä, G. Grassi, S. Rossi, J. Brandao De Melo, D. Oom, A. Branco and San-Miguel, *GHG Emissions of All World Countries*, p. 2023.
- 2 *Trends in Atmospheric Carbon Dioxide*, <https://gml.noaa.gov/ccgg/trends/weekly.html>, accessed 18 August 2024.
- 3 <https://www.climate.nasa.gov>, accessed 2024-08-18.
- 4 P. Markewitz, W. Kuckshinrichs, W. Leitner, J. Linssen, P. Zapp, R. Bongartz, A. Schreiber and T. E. Müller, *Energy Environ. Sci.*, 2012, **5**, 7281–7305.
- 5 X. Zhu, W. Xie, J. Wu, Y. Miao, C. Xiang, C. Chen, B. Ge, Z. Gan, F. Yang, M. Zhang, D. O'Hare, J. Li, T. Ge and R. Wang, *Chem. Soc. Rev.*, 2022, **51**, 6574–6651.
- 6 M. M. Jaffar, A. Rolfe, C. Brandoni, J. Martinez, C. Snape, S. Kaldis, A. Santos, B. Lysiak, A. Lappas, N. Hewitt and Y. Huang, *Carbon Capture Sci. Technol.*, 2024, **10**, 100179.
- 7 J. M. Kolle, M. Fayaz and A. Sayari, *Chem. Rev.*, 2021, **121**, 7280–7345.
- 8 S. Choi, J. H. Drese and C. W. Jones, *ChemSusChem*, 2009, **2**, 796–854.
- 9 M. J. Lashaki, S. Khiavi and A. Sayari, *Chem. Soc. Rev.*, 2019, **48**, 3320–3405.
- 10 <https://www.epa.gov/criteria-air-pollutants/naaqs-table>, accessed 18 August 2024.
- 11 <https://thundersaidenergy.com/downloads/air-quality-sulphur-nox-and-particulate-emissions/>, accessed 18 August 2024.
- 12 M. Wang, L. Yao, J. Wang, Z. Zhang, W. Qiao, D. Long and L. Ling, *Appl. Energy*, 2016, **168**, 282–290.
- 13 Y. Belmabkhout and A. Sayari, *Energy Fuels*, 2010, **24**, 5273–5280.
- 14 F. Rezaei and C. W. Jones, *Ind. Eng. Chem. Res.*, 2013, **52**, 12192–12201.
- 15 L. Kumar and S. K. Jana, *Rev. Chem. Eng.*, 2022, **38**, 843–880.
- 16 W. Li, C. Cheng, G. Gao, H. Xu, W. Huang, Z. Qu and N. Yan, *Mater. Horiz.*, 2024, **11**, 1889–1898.
- 17 P. Brandt, A. Nuhnen, M. Lange, J. Möllmer, O. Weingart and C. Janiak, *ACS Appl. Mater. Interfaces*, 2019, **11**, 17350–17358.
- 18 H. Yi, H. Deng, X. Tang, Q. Yu, X. Zhou and H. Liu, *J. Hazard. Mater.*, 2012, **203**, 111–117.
- 19 E. Ivanova and B. Koumanova, *J. Hazard. Mater.*, 2009, **167**, 306–312.
- 20 Y. Fu, Z. Wang, S. Li, X. He, C. Pan, J. Yan and G. Yu, *ACS Appl. Mater. Interfaces*, 2018, **10**, 36002–36009.
- 21 X. C. An, Z. M. Li, Y. Zhou, W. Zhu and D. J. Tao, *Chem. Eng. J.*, 2020, **394**, 124859.
- 22 J. Jia, P. M. Bhatt, S. R. Tavares, E. Abou-Hamad, Y. Belmabkhout, H. Jiang, A. Mallick, P. T. Parvatkar, G. Maurin and M. Eddaoudi, *Angew. Chem., Int. Ed.*, 2024, **63**, e202318844.
- 23 J. H. Jacobs, N. Chou, K. L. Lesage, Y. Xiao, J. M. Hill and R. A. Marriott, *Fuel*, 2023, **353**, 129239.
- 24 J. G. Bell, M. J. Benham and K. M. Thomas, *Energy Fuels*, 2021, **35**, 8102–8116.
- 25 A. A. Abdulrasheed, A. A. Jalil, S. Triwahyono, M. A. A. Zaini, Y. Gambo and M. Ibrahim, *Renew. Sustain. Energy Rev.*, 2018, **94**, 1067–1085.
- 26 F. H. Yang and R. T. Yang, *Carbon*, 2003, **41**, 2149–2158.
- 27 Y. L. Fan, H. P. Zhang, M. J. Yin, R. Krishna, X. F. Feng, L. Wang, M. B. Luo and F. Luo, *Inorg. Chem.*, 2021, **60**, 4–8.
- 28 Y. Zhang, P. Zhang, W. Yu, J. Zhang, J. Huang, J. Wang, M. Xu, Q. Deng, Z. Zeng and S. Deng, *ACS Appl. Mater. Interfaces*, 2019, **11**, 10680–10688.
- 29 G. L. Smith, J. E. Eyley, X. Han, X. Zhang, J. Li, N. M. Jacques, H. G. W. Godfrey, S. P. Argent, L. J. McCormick McPherson, S. J. Teat, Y. Cheng, M. D. Frogley, G. Cinque, S. J. Day, C. C. Tang, T. L. Easun, S. Rudić, A. J. Ramirez-Cuesta, S. Yang and M. Schröder, *Nat. Mater.*, 2019, **18**, 1358–1365.
- 30 R. Tailor, M. Abboud and A. Sayari, *Environ. Sci. Technol.*, 2014, **48**, 2025–2034.

- 31 R. Tailor, A. Ahmadalinezhad and A. Sayari, *Chem. Eng. J.*, 2014, **240**, 462–468.
- 32 R. Tailor and A. Sayari, *Chem. Eng. J.*, 2016, **289**, 142–149.
- 33 C. Kim, W. Choi and M. Choi, *ACS Appl. Mater. Interfaces*, 2019, **11**, 16586–16593.
- 34 A. Diaf, J. L. Garcia and E. J. Beckman, *J. Appl. Polym. Sci.*, 1994, **53**, 857–875.
- 35 H. C. Lan, J. Y. Zhang, Q. J. Dai, H. Ye, X. Y. Mao, Y. C. Wang, H. L. Peng, J. Du and K. Huang, *Chem. Eng. J.*, 2021, **409**, 127378.
- 36 H.-C. Lan, Y. T. Zou, Y. C. Wang, N. N. Cheng, W. L. Xu, H. L. Peng, K. Huang, L. Y. Kong and J. Du, *Chem. Eng. J.*, 2021, **422**, 129699.
- 37 L. L. Vasilieva, F. N. Dultsev and A. K. Milekhin, *J. Struct. Chem.*, 1996, **37**, 142–145.
- 38 G. Zhu, J.-M. Y. Carrillo, A. Sujana, C. N. Okonkwo, S. Park, B. G. Sumpter, C. W. Jones and R. P. Lively, *J. Mater. Chem. A*, 2018, **6**, 22043–22052.
- 39 W. Buijs, *Ind. Eng. Chem. Res.*, 2020, **59**, 13388–13395.
- 40 Y. Zhi, Y. Zhou, W. Su, Y. Sun and L. Zhou, *Ind. Eng. Chem. Res.*, 2011, **50**, 8698–8702.
- 41 H. Ziaei-Azad, J. M. Kolle, N. Al-Yasser and A. Sayari, *Microporous Mesoporous Mater.*, 2018, **262**, 166–174.
- 42 Y. Fan, Y. Q. Cai, X. Bin Fu, Y. Yao and Y. Chen, *Polymer*, 2016, **107**, 154–162.
- 43 M. Kruk, M. Jaroniec and A. Sayari, *Langmuir*, 1997, **13**, 6267–6273.
- 44 X. Yan, L. Zhang, Y. Zhang, G. Yang and Z. Yan, *Ind. Eng. Chem. Res.*, 2011, **50**, 3220–3226.
- 45 A. von Harpe, H. Petersen, Y. Li and T. Kissel, *J. Control. Release*, 2000, **69**, 309–322.
- 46 D. R. Holycross and M. Chai, *Macromolecules*, 2013, **46**, 6891–6897.
- 47 A. Sayari, Y. Belmabkhout and E. Da'na, *Langmuir*, 2012, **28**, 4241–4247.
- 48 H. T. Vo, S. H. Cho, U. Lee, J. Jae, H. Kim and H. Lee, *J. Ind. Eng. Chem.*, 2019, **69**, 338–344.
- 49 H. J. Lee, S. R. Lim, K. I. Lee, C. S. Kim, H. S. Kim, J. S. Choi and S. D. Lee, *US Pat.*, US8894956, 2014.